UC San Diego
UC San Diego Previously Published Works

Title
Identifying transport behavior of single-molecule trajectories.

Permalink
https://escholarship.org/uc/item/24s6j48x

Journal
Biophysical journal, 107(10)

ISSN
0006-3495

Authors
Regner, Benjamin M
Tartakovsky, Daniel M
Sejnowski, Terrence J

Publication Date
2014-11-01

DOI
10.1016/j.bpj.2014.10.005

Peer reviewed

Article

Identifying Transport Behavior of Single-Molecule Trajectories

Benjamin M. Regner,[1,2,*] Daniel M. Tartakovsky,[1] and Terrence J. Sejnowski[2,3]

[1]Department of Mechanical and Aerospace Engineering and [2]Division of Biological Studies Sciences, University of California at San Diego, La Jolla, California; and [3]Howard Hughes Medical Institute, Salk Institute for Biological Studies, La Jolla, California

ABSTRACT Models of biological diffusion-reaction systems require accurate classification of the underlying diffusive dynamics (e.g., Fickian, subdiffusive, or superdiffusive). We use a renormalization group operator to identify the anomalous (non-Fickian) diffusion behavior from a short trajectory of a single molecule. The method provides quantitative information about the underlying stochastic process, including its anomalous scaling exponent. The classification algorithm is first validated on simulated trajectories of known scaling. Then it is applied to experimental trajectories of microspheres diffusing in cytoplasm, revealing heterogeneous diffusive dynamics. The simplicity and robustness of this classification algorithm makes it an effective tool for analysis of rare stochastic events that occur in complex biological systems.

INTRODUCTION

Stochastic fluctuations arise in biological systems at all length and timescales. An example is the diffusion of biomolecules, driven by thermal fluctuations, providing transport for biochemical processes. A familiar process that can generate such behavior is Brownian motion, although in biological systems the explicit assumption that particles are dilute is often violated. Diffusion processes that do not produce Brownian statistics are said to exhibit anomalous (non-Fickian) diffusion. Occurrence of anomalous diffusion has been reported in diverse phenomena, and has enriched understanding of biological systems (1).

Particle trajectories produced by single-molecule experiments are particularly suitable for characterizing biological diffusion behavior. A particle trajectory consists of M locations $X_i = X(t_i)$, which the particle occupies at times $t = t_i$. This trajectory is represented by a sequence of time-ordered random variables

$$\mathbf{X} = \{X_i\}_{i=0}^{M}.$$

Anomalous behavior arises when a trajectory has nonzero drift, correlated increments, nonstationary increments, or some combination (2). Equivalently, Brownian motion is observed when these conditions are absent. The trajectory of a particle undergoing Brownian motion exhibits a mean-square displacement (MSD) that grows linearly with time t. Anomalous diffusion typically produces an MSD, $\langle \mathbf{X}^2 \rangle$, which is a nonlinear function of t, e.g., a power law

$$\langle \mathbf{X}^2 \rangle(t) = D_\alpha t^\alpha, \qquad 0 < \alpha < 2, \tag{1}$$

Here D_α is the diffusion coefficient, and $\langle \cdot \rangle$ denotes an average over an ensemble of random trajectories. For stationary processes considered in this analysis, the exponent α is assumed constant throughout the time-course. The process $\mathbf{X}$ is called subdiffusive if the exponent $\alpha < 1$, and superdiffusive if exponent $\alpha > 1$ (3). A time-averaged MSD (TAMSD) can be used to analyze single trajectories and is defined for the ith trajectory by

$$\overline{\mathbf{X}_i^2}(\Delta, t) = \frac{1}{t - \Delta} \int_0^{t-\Delta} [\mathbf{X}_i(t' + \Delta) - \mathbf{X}_i(t')]^2 dt', \tag{2}$$

where Δ is a lag time (4).

Although many experiments use TAMSD as a key statistic characterizing the observed dynamics, a number of studies have demonstrated that it can be a problematic metric for classification in certain cases (2,5,6). In response, a number of algorithms have been proposed for process classification, such as p-variation (7), autocorrelation functions (8), higher order moments (9), and an ergodicity breaking parameter (10). Alternatively, approaches have been developed with a focus on experimental trajectories using empirical evidence of deviation from Brownian motion (11–13).

A recently proposed framework based on a renormalization group operator (RGO) (2,14,15) provides a promising alternative. A random trajectory $\mathbf{X}$ has a set of increments $\mathbf{I} = \{I_i\}_{i=0}^{M}$, with each increment computed as $I_i = X_{i+1} - X_i$. An RGO $R_{p,n}$ can be defined by

$$(R_{p,n}\mathbf{I})_i \equiv \sum_{k=in}^{(i+1)n-1} \frac{I_k}{n^p}, \qquad p > 0, \qquad n \geq 1, \tag{3}$$

and a new replica trajectory $\mathbf{J}$ is determined as $J^{p,n}{}_i = (R_{p,n}\mathbf{I})_i$. For a fixed p, a sequence $\mathbf{I}$ is called a fixed point of the RGO if the relationship

$$\mathbf{J}^{p,n} \overset{d}{=} \mathbf{I} \qquad (4)$$

holds for all $n \geq 1$, where $\overset{d}{=}$ means equal in distribution (16). A process that is a fixed point with scaling p is said to be p-diffusive, or p-self-similar, and is related to the anomalous diffusion exponent by $\alpha = 2p$ (2). A generalization is a random RGO, in which the scaling is a random variable P (14). In this framework, a single experimental trajectory is a realization of a process that samples a scaling distribution $f_P(p)$. Here, we propose an algorithm to determine the anomalous diffusion exponent distribution $f_P(p)$ of a stochastic trajectory. The goal is to obtain $\overline{p}$ from single, short trajectories of experimental data; other methods may be more appropriate for analytic processes (17).

METHODS

Classification algorithm

The proposed algorithm consists of the following four steps:

1. A single trajectory $\mathbf{X}$ is transformed into the increment process $\mathbf{I}$ and the empirical cumulative distribution function (CDF), $F_I^0(x)$, of $\mathbf{I}$ is computed.

2. A constrained optimization is performed on a goodness-of-fit statistic comparing empirical CDFs. Although other options exist, good results were found by minimizing the goodness-of-fit statistic from Kuiper's two-sample test (18),

$$g^{P,n} = \sup_x \left| F_I^0(x) - F_J^{P,n}(x) \right| - \inf_x \left| F_I^0(x) - F_J^{P,n}(x) \right|, \quad (5)$$

where $F^{P,n}{}_J(x)$ is an empirical CDF of $\mathbf{J}^{P,n} = R_{p,n}\mathbf{I}$.

3. Optimization is repeated for many values of n to obtain corresponding best-fit values of p and are plotted as a histogram to obtain a distribution $f_P(p)$ for a given realization.

4. The scaling exponent is computed as $\alpha = 2\overline{p}$, where $\overline{p}$ is the mean of the empirical distribution f_P; the corresponding diffusion coefficient is defined by $D_\alpha = \sigma^2{}_I/(2\delta t^\alpha d)$, where $\sigma^2{}_I(t)$ is the variance of $\mathbf{I}$, δt is the time step, and d is the spatial dimension (19).

The use of increments $I^\Delta{}_i = X_{i+\Delta} - X_i$ for a lag time Δ (the number of time steps) improves estimation of D_α. The diffusion coefficient is then calculated as

$$D_\alpha = \frac{1}{M} \sum_{\Delta=1}^{M} \frac{\sigma^2_{I\Delta}(t)}{2d(\Delta\delta t)^\alpha}. \qquad (6)$$

This calculation also acts as an indicator of the accuracy of the calculated scaling. If an estimate of $\overline{p}$ is inaccurate, then $D_\alpha(\Delta)$ will change significantly with Δ, indicating a poor fit.

A trivial extension is to perform the operation over a population of trajectories to produce an ensemble distribution. This is analogous to other methods of computing the average scaling, but has the advantage that each trajectory is treated individually, a fact particularly useful when the population contains a mixture of processes. Further refinements, such as subdividing the trajectories into subtrajectories or performing a moving window analysis, can be used to obtain information local in time.

Stochastic processes

Several stochastic processes are used below to validate the proposed algorithm. Brownian motion $\mathbf{B}_t$ is a time series of Gaussian-distributed random variables with zero mean and unit variance. A Lèvy flight $\mathbf{L}_t$ can be generated by taking step increments from a stable distribution $S(\alpha_L,\beta,0)$ with $\beta = 0$ (20). Note the distribution parameter α_L is different from the anomalous diffusion exponent α. The analytical MSD of $\mathbf{L}_t$ scales like t^{2/α_L}, and is therefore $1/\alpha_L$-diffusive (21). Fractional Brownian motion (fBM) is denoted $\mathbf{B}^H{}_t$ and defined with initial condition $B^H{}_0 = 0$, zero mean $\langle \mathbf{B}^H{}_t \rangle = 0$, and a two-point correlation,

$$\langle \mathbf{B}^H_t \mathbf{B}^H_s \rangle = \left(|t|^{2H} + |s|^{2H} - |t-s|^{2H} \right)/2,$$

where H is the Hurst exponent. In this work, fBM is simulated using the circulant method as implemented in the R package dvfBm (22,23). It can be shown that $\mathbf{B}^H{}_t$ is H-diffusive.

RESULTS

Validation

The proposed classification scheme produces a distribution of scaling exponents for each individual trajectory, and provides an estimate of the mean and variance from the single-trajectory scaling distribution $f_P(p)$. In Fig. 1, trajectories generated by three stochastic processes described above are analyzed using the TAMSD and compared to the proposed RGO method. Ensemble averages ($N = 10^5$) are shown as a dashed line. In all cases, the use of the RGO method reduces the dispersion of the estimated scaling. Fig. 1 *a* exhibits the $\mathbf{B}_t$ trajectories computed with TAMSD (*black*) and the RGO algorithm (*gray*). A similar comparison for $\mathbf{B}^H{}_t$ is provided in Fig. 1 *b* for $H = 0.25$ and 0.75. For $H = 0.25$, the RGO method (*light blue*) converges to the ensemble mean much more slowly than TAMSD (*dark blue*), whereas the convergence rates of TAMSD (*dark orange*), and RGO (*light orange*) are nearly identical for $H = 0.75$. In Fig. 1 *c*, the TAMSD analysis of $\mathbf{L}_t$ for $\alpha_L = 0.5$ and 1.0 incorrectly predicts a scaling of $p = 0.5$ (*dark purple*) compared to the analytically derived scaling $p = 1/\alpha_L$ (24). The RGO method correctly characterizes the trajectories for $\alpha_L = 0.5$ (*green*) and 1.0 (*light purple*).

A subtle point is determining the limits of accurately characterizing a stochastic trajectory. Jeon et al. (25) introduced an ergodicity-breaking parameter

$$\xi_i = \overline{X_i^2} \Big/ \left\langle \overline{X^2} \right\rangle$$

as a means of analysis of pre-ergodic data. Previously, we used this parameter to distinguish between stochastic processes (26). Fig. 2 exhibits the mean $\overline{\xi}$ obtained with such analysis for $\mathbf{B}_t$ and $\mathbf{B}^H{}_t$. It shows weak ergodicity breaking for short ($M < 100$) trajectories, which is in agreement with the weak ergodicity breaking at short times previously observed for $\mathbf{B}^H{}_t$ (27). This is also true for $\mathbf{B}_t$, an ergodic process, suggesting there is insufficient information in a short trajectory to accurately characterize the underlying
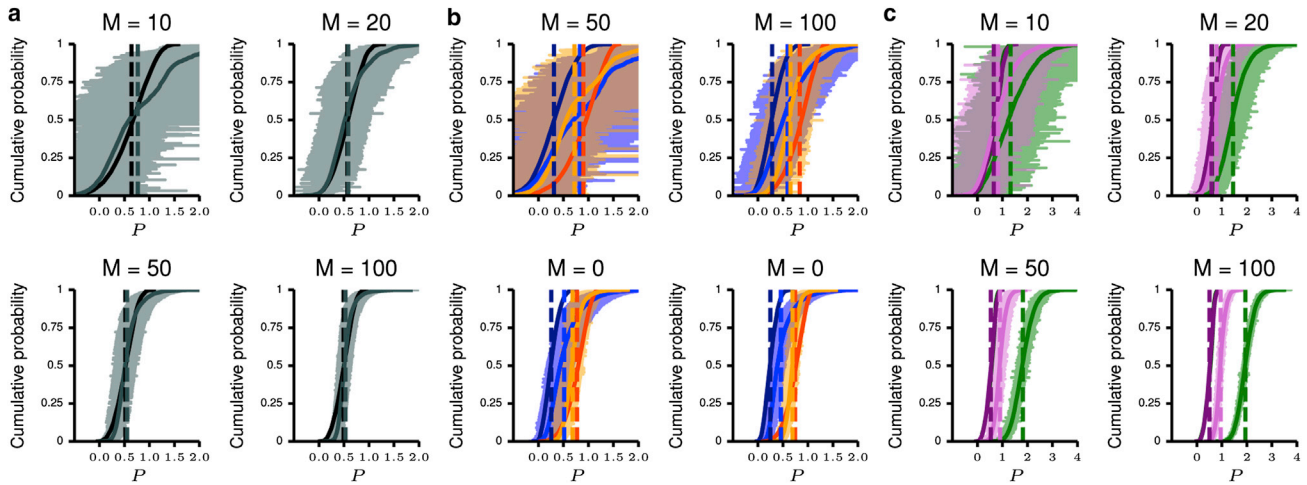
FIGURE 1 Empirical cumulative distribution of *p* estimated from single trajectories. The anomalous diffusion exponent *p* is estimated using the TAMSD and the proposed RGO method from single trajectories of length *M*. Distributions are computed from $N = 10^5$ realizations. (*Dashed lines*) Ensemble average for each method. (*a*) $\mathbf{B}_t$ trajectories are analyzed using TAMSD (*black*) and the RGO method (*gray*). The standard error for each trajectory estimate is plotted for the RGO case, but cannot be computed using TAMSD. A small decrease in dispersion is seen using the RGO method. (*b*) $\mathbf{B}_t^H$ trajectories are analyzed for two values of $H = 0.25$ and 0.75. The TAMSD method produces a more accurate ensemble average for $H = 0.25$ (*dark blue*) in comparison to the RGO method (*light blue*). In the case of $H = 0.75$, both TAMSD (*dark orange*) and RGO (*light orange*) have similar performance, with the RGO method producing less dispersion. (*c*) $\mathbf{L}_t$ trajectories are analyzed for two scalings $\alpha_L = 0.5$ and 1 ($p = 2.0$ and 1.0). Importantly, the TAMSD (*dark purple*) computes an incorrect scaling of $p = 0.5$ for both $\alpha_L = 0.5$ (*green*) and $\alpha_L = 1$ (*light purple*), which the RGO method accurately characterizes.

process. Therefore, an accurate determination of the anomalous scaling exponent from single-trajectory data is undermined by the scarcity of data and pre-ergodic convergence associated with short trajectories.

Experimental data typically consist of a few trajectories that are short in time. Ten realizations of $\mathbf{B}_t^H$ are simulated with $H = 0.25$ and 0.75, for $M = 1000$ time steps. Their representative distributions f_P are shown in Fig. 3, *a* and *b*, for $H = 0.25$ and $H = 0.75$, respectively. In all cases, good agreement with the scaling of the underlying process is observed. The exact scaling, $\delta(x - P)$, where δ is the Dirac delta function,

is replaced with a finite-width distribution that accounts for uncertainty introduced by the trajectory's short length. An ensemble histogram of the population of 10 trajectories with $H = 0.25$ in Fig. 3 *c* shows weak convergence to the expected mean. A mixed population of 10 trajectories from each H in Fig. 3 *d* demonstrates that the algorithm robustly
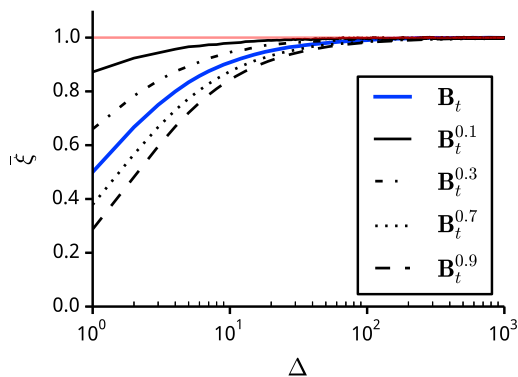

FIGURE 2 Pre-ergodic analysis of stochastic processes. The mean $\bar{\xi}$ of the ergodicity parameter distribution $\phi(\xi)$ is plotted against lag time Δ. A comparison is made between Brownian motion and fractional Brownian motion with several Hurst exponents. Importantly, these processes show weak ergodicity breaking in a pre-ergodic regime. This limits accurate classification of short ($M < 100$) single trajectories generated by these processes. To see this figure in color, go online.
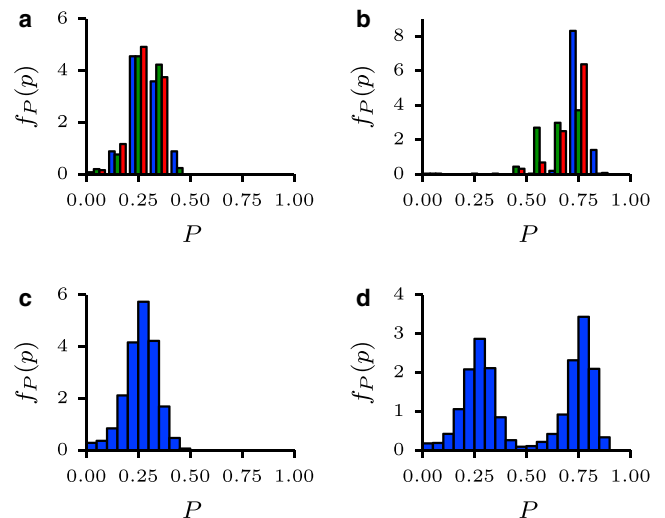

FIGURE 3 RGO analysis of fBM data. Ten trajectories of a fractional Brownian motion $\mathbf{B}_t^H$ are simulated for $H = 0.25$ and $H = 0.75$ over 1000 time steps. Our algorithm is applied to these trajectories to obtain distributions of the critical exponent *P*. (*a* and *b*) Single-trajectory histograms for $H = 0.25$ and $H = 0.75$, respectively. (*c*) Ensemble histogram from a population of 10 trajectories with $H = 0.25$. (*d*) Ensemble histogram of all trajectories combined, revealing an expected bimodal distribution that ensemble methods would fail to detect.

recovers a bimodal distribution for the mixture case without additional constraints on the algorithm.

Experimental data analysis

The validated classification algorithm is used to analyze previously reported data (26). Briefly summarizing, we obtained three-dimensional particle trajectories of a fluorescent microsphere, diameter 1 μm, diffusing in a cellular extract prepared from *Xenopus* oocytes. Another set of trajectories was also obtained from the same extract treated with nocodazole, which is known to depolymerize microtubules. For all experiments, the total acquisition time per three-dimensional volume was 86 ms. Previously, an MSD-based analysis, using Eq. 1, classified transport as superdiffusive along microtubules in the extract case ($\alpha = 1.5$ for both short and long times; and $D_\alpha = 0.014$ and 0.038 in short- and long-time analyses). The units for all experimental diffusion coefficients are μm^2/s$^\alpha$, in agreement with Eq. 1. Addition of nocodazole led to subdiffusive transport at short times ($\alpha = 0.6$), and classical diffusion ($\alpha = 1.0$) at long times; in both cases, $D_\alpha = 0.16$ (26). Fig. 4 exhibits the resulting MSDs.

Fig. 5 presents the results obtained with our classification algorithm for the extract (*left column*) and nocodazole (*right column*) cases. Distributions from single representative trajectories are shown in Fig. 5, *a* and *b*. Both cases exhibit
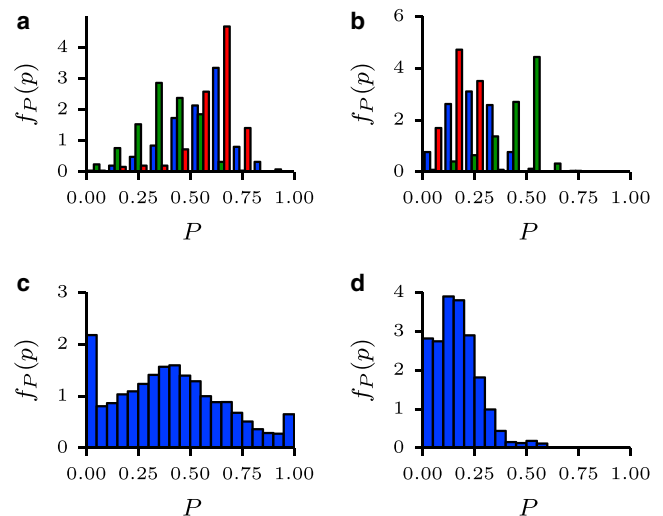
FIGURE 5 RGO analysis of experimental data. (*a* and *b*) Representative histograms of the empirical scaling distribution $f_P(p)$ of individual trajectories from the extract and nocodazole cases, respectively. Three examples are shown with each color indicating results from a single trajectory. (*c* and *d*) Ensemble histograms for the two cases. In the extract case, subdiffusive behavior is observed, which was not indicated by the MSD analysis. Similarly, weak superdiffusive behavior is observed in the nocodazole case, suggesting incomplete depolymerization of microtubules. The large mass at $P = 0$ is due to occasional calculation of negative scaling exponents due to short trajectory size, but physical processes have the constraint $p > 0$.

superdiffusive and subdiffusive signatures, although they are less evident in the nocodazole case. These results indicate that the experimentally observed trajectories are characterized by process transitions. In the extract case this is not surprising, inasmuch as the dynamics of microtubule transport include rapid switching between on- and off-states as the microsphere interacts with the microtubules (28).

Superdiffusive transport in the nocodazole case suggests incomplete depolymerization of the microtubules, which remained undetected by the MSD analysis. Fig. 5, *c* and *d*, shows ensemble population distributions, with $N = 38$ in the extract case and $N = 19$ in the nocodazole case. In the extract case, multiple scalings occur during the time course of the collected data. The ensemble distributions reveal that in the case of nocodazole, whereas the majority of trajectories undergo subdiffusion, there is a strong signature of superdiffusive transport. Table 1 contains the values of the diffusion coefficient D_α computed with Eq. S1. The MSD and RGO methods predict similar values of D_α, with the small disagreement attributed to the MSD's use of Eq. 1, in which D_α is sensitive to the fitting of α.

Comparison to previous methods

Applying the renormalization group method using a moving window provides a useful comparison to alternative characterization methods. In this case, we compare $\alpha/2$ from the classic TAMSD method, the *Dev* parameter derived by
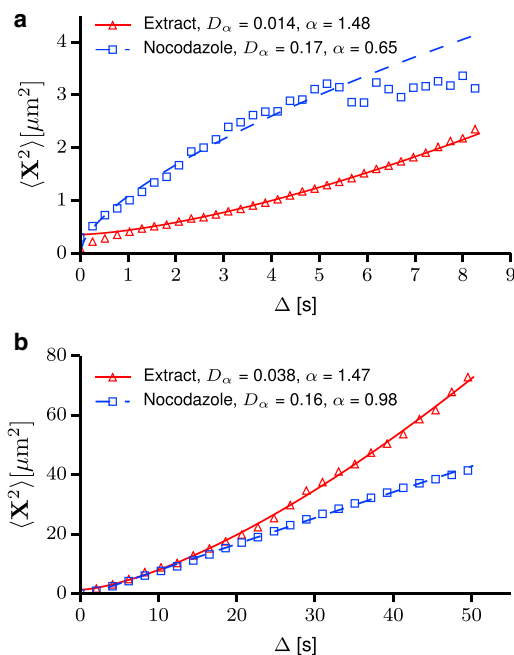

FIGURE 4 Ensemble MSD of individual TAMSDs from each experimental trajectories. (*a*) At short times, transport is superdiffusive in the extract case (due to active transport along microtubules) and subdiffusive in the nocodazole case. (*b*) At long times, transport is superdiffusive in the extract case and Fickian in the nocodazole case. To see this figure in color, go online.

TABLE 1 Diffusion coefficients calculated with the MSD and RGO methods for different time windows

	Short time D_α		Long time D_α	
	MSD	RGO	MSD	RGO
Extract	0.014	0.029	0.038	0.046
Nocodazole	0.16	0.043	0.17	0.126

Units are $\mu m^2/s^\alpha$.

Huet et al. (11), and a velocity correlation parameter *SCI* derived by Bouzigues and Dahan (11,13). We compare this with the mean scaling $\overline{p}$ and the evolution of the full distribution $f_P(p)$ over time. In all cases a window size of 41 time points is used.

A comparison is first made using simulated data of known scaling. The simulated trajectory is a concatenation of three distinct walks, each with 200 time steps:

1. A fractional Brownian motion with $H = 0.25$,
2. A fractional Brownian motion with $H = 0.75$, and
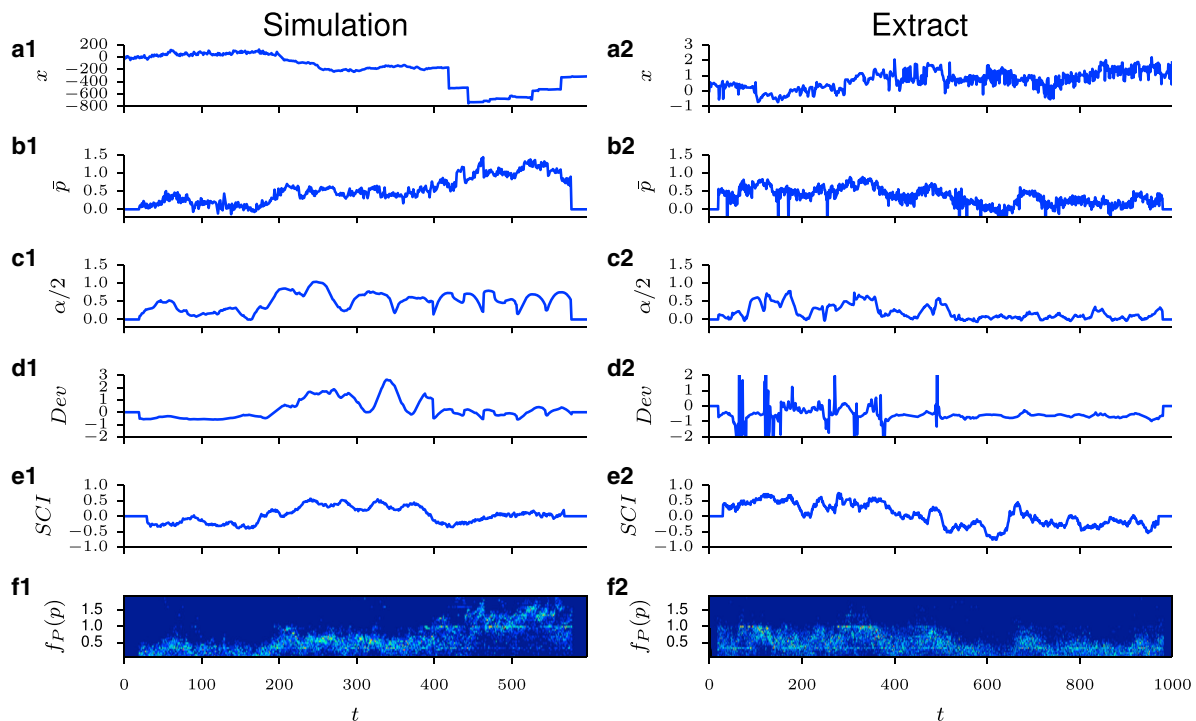3. A Lèvy flight with $\alpha_L = 1$.

The computed characterization is shown in Fig. 6 in the left column (*Simulation*). The TAMSD method works well for the fBM cases, but fails to find the correct scaling for the

Lévy flight, as expected from Fig. 1. The mean $\overline{p}$ is noisy, but varies around the expected scaling for each distinct process. The parameter *Dev* gives some qualitative information, but it is not clear how to map *Dev* to the actual scaling exponent. This method also fails to distinguish a Lévy flight. The correlation *SCI* only gives a rough qualitative sense of the change in underlying scaling, but no quantitative information. Finally, the full distribution $f_P(p)$ gives a good sense of the local fluctuations around the underlying scaling exponent, despite containing limited samples per time point due to the small window size.

These methods are also applied to one experimental trajectory shown in the right column (*Extract*) of Fig. 6. In this case, similar features are seen to the simulation case, although the parameters are noisier due to particle location uncertainty in experimental data. The particle appears to undergo Brownian motion in the beginning of the trajectory, switching to subdiffusive behavior at ~500–600 time points.

CONCLUSION

We have shown that renormalizaion group operators are an effective method for determining the scaling exponent of

FIGURE 6 Moving window analysis of simulated and extract trajectories. (*a*1) Simulated trajectory; first 200 points are a fractional Brownian motion with $H = 0.25$, the next 200 points are an fBM with $H = 0.75$, and the last 200 points are a Lévy flight with $\alpha_L = 1$. All moving windows for the analysis of this trajectory uses a window size of 41. (*a*2) Experimental trajectory of microsphere diffusing in cellular extract. (*b*1,2) The mean value $\overline{p}$ computed using the proposed algorithm. (*c*1,2) $\alpha/2$ calculated using a moving window time-averaged mean-squared displacement analysis. (*d*1,2) The parameter *Dev* proposed by Huet et al. (11). (*e*1,2) The parameter *SCI* proposed by Bouzigues and Dahan (13). (*f*1,2) The full distribution $f_P(p)$ computed using the proposed algorithm. Although the distributions are sparsely populated due to the small window size, the random scaling for each process as it varies with time is clearly shown. In the extract case, the distribution suggests Brownian motion in the initial segment followed by a transition to subdiffusive behavior of ~500–600 time points. To see this figure in color, go online.

discrete stochastic processes and experimental data. The analysis suggests that whereas fluctuations in short-time windows can produce improbable sequences that scale differently from the underlying process, their average behavior is sufficient to correctly estimate the scaling exponent and to classify the process. Many biological phenomena are characterized by broad distributions for which it may be difficult (or even inappropriate) to assign a single value of the scaling exponent α. The observed distributions are likely generated by process transitions, which reflect the presence of multiple transport mechanisms (e.g., free diffusion, varieties of cytoskeletal transport, and active transport through pores) that may act upon biomolecules during different time windows or events (29). From a regulatory perspective, diverse transport mechanisms with different scaling would provide a powerful means of control over biochemical pathways. The assortment of scalings seen in Fig. 5 is evidence of diversity in microtubule transport. The MSD analysis of individual trajectories of diffusing chromosomal loci (30) provides further support for this conclusion. The MSD-based estimates of the scaling exponents for individual trajectories were collected into a histogram shown in Fig. 2 a of Javer et al. (30). It is similar to the histogram for the extract case shown in Fig. 5 c. The proposed algorithm could also be used to classify the distinct short-time diffusive behaviors observed in different subcellular regions reported by Javer et al. (30).

Nonstationary transport has been previously observed in the cytoplasm and plasma membrane of living cells (31,32), in which the distribution of anomalous diffusion exponents was a function of time and the process generating the dynamics, i.e., $f_P(p|t,\mathbf{A}_t)$, where $\mathbf{A}_i$ is a specific stochastic process. Here, we have assumed that the dynamics are stationary over the acquisition time, so the anomalous exponent is only a function of the generating stochastic process $f_P(p \mid \mathbf{A}_t)$. In previous experiments, nonstationary behavior was apparent on a timescale of 100 s (31), similar to the timescale of the experiments presented here. Therefore, we are at the limit of applicability of the proposed method for stationary processes. However, classifying nonstationary processes using short trajectories is ill-posed in many cases, due to a combination of limited statistical information and an unknown rate of change in dynamics. Without sufficient accumulation of statistical information, i.e., many time points, accurately classifying such a process would be difficult at best. In addition, the proposed method does not properly characterize fundamentally nonstationary processes. Assuming sufficient data, a similar method to the one proposed here could be developed using a different RGO, similar to previous analytical work (17), but the details remain unresolved.

In summary, we developed a classification technique to analyze short trajectories of a single biomolecule based on an RGO (2), which allows computing both the anomalous scaling exponent and diffusion coefficient of a biomolecule's motion. The RGO-based classification alleviates key impediments to accurate identification of anomalous transport, which stem from scarcity of observed biomolecule trajectories, short duration of observation, and measurement errors. After validation on simulated stochastic processes, we used the proposed method to analyze trajectories of diffusing microspheres observed in several biological environments. The RGO approach identified multiple transport processes affecting the observed particle migration, revealing behavior that had been missed in a previous analysis. The RGO method could be used to analyze single trial data from other sources in which transitions are likely to occur.

REFERENCES

1. Höfling, F., and T. Franosch. 2013. Anomalous transport in the crowded world of biological cells. *Rep. Prog. Phys.* 76:046602.

2. O'Malley, D., and J. H. Cushman. 2012. A renormalization group classification of nonstationary and/or infinite second moment diffusive processes. *J. Stat. Phys.* 146:989–1000.

3. Bouchaud, J.-P., and A. Georges. 1990. Anomalous diffusion in disordered media: statistical mechanisms, models and physical applications. *Phys. Rep.* 195:127–293.

4. Qian, H., M. P. Sheetz, and E. L. Elson. 1991. Single particle tracking. Analysis of diffusion and flow in two-dimensional systems. *Biophys. J.* 60:910–921.

5. Kepten, E., I. Bronshtein, and Y. Garini. 2013. Improved estimation of anomalous diffusion exponents in single-particle tracking experiments. *Phys. Rev. E Stat. Nonlin. Soft Matter Phys.* 87:052713.

6. Michalet, X. 2010. Mean square displacement analysis of single-particle trajectories with localization error: Brownian motion in an isotropic medium. *Phys. Rev. E Stat. Nonlin. Soft Matter Phys.* 82:041914.

7. He, Y., S. Burov, …, E. Barkai. 2008. Random time-scale invariant diffusion and transport coefficients. *Phys. Rev. Lett.* 101:058101.

8. Min, W., G. Luo, …, X. S. Xie. 2005. Observation of a power-law memory kernel for fluctuations within a single protein molecule. *Phys. Rev. Lett.* 94:198302.

9. Gal, N., and D. Weihs. 2010. Experimental evidence of strong anomalous diffusion in living cells. *Phys. Rev. E Stat. Nonlin. Soft Matter Phys.* 81:020903.

10. Magdziarz, M., A. Weron, …, J. Klafter. 2009. Fractional Brownian motion versus the continuous-time random walk: a simple test for subdiffusive dynamics. *Phys. Rev. Lett.* 103:180602.

11. Huet, S., E. Karatekin, …, J.-P. Henry. 2006. Analysis of transient behavior in complex trajectories: application to secretory vesicle dynamics. *Biophys. J.* 91:3542–3559.

12. Arcizet, D., B. Meier, …, D. Heinrich. 2008. Temporal analysis of active and passive transport in living cells. *Phys. Rev. Lett.* 101:248103.

13. Bouzigues, C., and M. Dahan. 2007. Transient directed motions of $GABA_A$ receptors in growth cones detected by a speed correlation index. *Biophys. J.* 92:654–660.

14. O'Malley, D., and J. H. Cushman. 2012. Random renormalization group operators applied to stochastic dynamics. *J. Stat. Phys.* 149:943–950.

15. Park, M., D. O'Malley, and J. H. Cushman. 2014. Generalized similarity, renormalization groups, and nonlinear clocks for multiscaling. *Phys. Rev. E Stat. Nonlin. Soft Matter Phys.* 89:042104.

16. Samorodnitsky, G., and M. S. Taqqu. 1994. Stable Non-Gaussian Random Processes: Stochastic Models with Infinite Variance, 1st Ed. Chapman and Hall/CRC, Boca Raton, FL.

17. O'Malley, D., and J. H. Cushman. 2012. Two-scale renormalization-group classification of diffusive processes. *Phys. Rev. E Stat. Nonlin. Soft Matter Phys.* 86:011126.

18. Kuiper, N. H. 1960. Tests concerning random points on a circle. *Koninklijke Nederlandse Akademie van Wetenschappen Proc. A.* 63:38–47.

19. Metzler, R., and J. Klafter. 2000. The random walk's guide to anomalous diffusion: a fractional dynamics approach. *Phys. Rep.* 339:1–77.

20. Nolan, J. P. 2014. Stable Distributions—Models for Heavy Tailed Data. Birkhauser, Boston, MA. Chapter 1 online at http://academic2.american.edu/~jpnolan/stable/chap1.pdf.

21. Zanette, D. H. 1999. Statistical-thermodynamical foundations of anomalous diffusion. *Braz. J. Phys.* 29:108–124.

22. Wood, A. T. A., and G. Chan. 1994. Simulation of stationary Gaussian processes in [0, 1] *d. J. Comput. Graph. Stat.* 3:409–432.

23. Coeurjolly, J.-F. 2009. DVFBM: Discrete Variations of a Fractional Brownian Motion. R Package ver. 1.0. http://CRAN.R-project.org/package=dvfBm.

24. Ghaemi, M., Z. Zabihinpour, and Y. Asgari. 2009. Computer simulation study of the Levy flight process. *Physica A.* 388:1509–1514.

25. Jeon, J.-H., and R. Metzler. 2010. Analysis of short subdiffusive time series: scatter of the time-averaged mean-squared displacement. *J. Phys. A Math Theor.* 43:252001.

26. Regner, B. M., D. Vučinić, …, T. J. Sejnowski. 2013. Anomalous diffusion of single particles in cytoplasm. *Biophys. J.* 104:1652–1660.

27. Deng, W., and E. Barkai. 2009. Ergodic properties of fractional Brownian-Langevin motion. *Phys. Rev. E Stat. Nonlin. Soft Matter Phys.* 79:011112.

28. Alberts, B., A. Johnson, …, P. Walter. 2008. Molecular Biology of the Cell. Garland Science, New York.

29. Friedman, M. H. 2008. Principles and Models of Biological Transport. Springer, New York.

30. Javer, A., Z. Long, …, M. Cosentino Lagomarsino. 2013. Short-time movement of E. coli chromosomal loci depends on coordinate and subcellular localization. *Nat. Comm.* 4:3003.

31. Tabei, S. M., S. Burov, …, N. F. Scherer. 2013. Intracellular transport of insulin granules is a subordinated random walk. *Proc. Natl. Acad. Sci. USA.* 110:4911–4916.

32. Weigel, A. V., B. Simon, …, D. Krapf. 2011. Ergodic and nonergodic processes coexist in the plasma membrane as observed by single-molecule tracking. *Proc. Natl. Acad. Sci. USA.* 108:6438–6443.